



Exsolution of multimetallic particles from high-entropy oxides for CO₂ hydrogenation to methanol

Guilherme B. Strapasson^{1,2,3,*}, Larissa E. R. Ferreira¹, Emma S. Chaos³, Adrian S. Arjona³, Silma A. Correa⁴, Cristiane B. Rodella², Kirsten M. Ø. Jensen³, Andrea Kirsch³, Daniela Zanchet¹

- ¹Institute of Chemistry, University of Campinas, Campinas, Brazil
- ²Brazilian Synchrotron Light Laboratory, CNPEM, Campinas, Brazil
- ³Department of Chemistry, University of Copenhagen, Copenhagen, Denmark
- ⁴Institute of Chemistry, Universidade Federal do Rio Grande do Sul, Porto Alegre, Brazil

Resumo/Abstract

RESUMO – Este trabalho apresenta a síntese e avaliação catalítica de um óxido espinélio de alta entropia (Co_{0.33}Ni_{0.33}Cu_{0.33})(Cr_{0.5}Mn_{0.5})₂O₄ como plataforma para a exsolução *in situ* de nanopartículas multimetálicas ativas na hidrogenação de CO₂ a metanol. A caracterização estrutural revelou a exsolução dependente da temperatura de Cu, Ni e Co, formando nanopartículas com diferentes tamanhos e composições, desde ricas em Cu até ligas CuNiCo. Testes catalíticos realizados a 100 bar e 200 °C mostraram que a redução moderada (500 °C) resultou no melhor equilíbrio entre atividade e seletividade, com rendimento de metanol de 1,5%; enquanto temperaturas mais altas diminuíram a atividade, mas aumentaram a seletividade para álcoois. Esses resultados destacam o potencial dos óxidos de alta entropia como catalisadores versáteis e moduláveis para o desenvolvimento de materiais termicamente estáveis e seletivos na conversão de CO₂.

Palavras-chave: Hidrogenação de CO₂, Nanomateriais, Óxidos de alta entropia, Exsolução

ABSTRACT – This work reports the synthesis and catalytic evaluation of a high-entropy spinel oxide (Co_{0.33}Ni_{0.33}Cu_{0.33})(Cr_{0.5}Mn_{0.5})₂O₄ as a platform for *in situ* exsolution of multimetallic nanoparticles active in CO₂ hydrogenation to methanol. Structural characterization revealed temperature-dependent exsolution of Cu, Ni, and Co, forming nanoparticles with variable size and composition, from Cu-rich to CuNiCo alloyed phases. Catalytic tests at 100 bar and 200 °C showed that moderate reduction (500 °C) led to the best compromise between activity and selectivity, with a methanol yield of 1.5%; whereas higher temperatures reduced activity but increased alcohols selectivity. These results highlight the potential of high-entropy oxides as versatile and tunable catalysts for designing thermally stable and selective catalysts for CO₂ conversion. *Keywords: CO₂ hydrogenation, Nanomaterials, High Entropy Oxides, Exsolution*

Introduction

The catalytic hydrogenation of CO₂ to methanol represents a strategic solution for reducing greenhouse gas emissions while producing valuable added chemicals. While Cu/ZnO/Al₂O₃ remains the industrial benchmark for this reaction, the development of alternative catalyst systems with enhanced activity, selectivity, and long-term stability has become an increasingly important goal in the search for more sustainable and efficient catalytic systems. Among the strategies being explored, the in situ exsolution of nanoparticles from oxide matrices has emerged as a powerful method for constructing catalytically active metaloxide interfaces with improved thermal stability (1-3). However, most research remains limited to low-doped perovskite-type oxides, typically composed of less than 20 at.% of the exsolvable cation. Over 80% of these studies focus on perovskites, with Ni being the most widely studied exsolvable metal (>50%) (4). Exsolution of Cu or Cu-based alloys, despite their high activity in CO2 hydrogenation, is reported in less than 5% of cases (5), and exsolution from

other crystal structures, such as spinels, accounts for less than 2% (4).

While extrinsic factors such as temperature, gas composition, and reduction time influence the exsolution process (4,6), intrinsic properties of the host oxide, such as strain, cation coordination, and defect chemistry, are fundamental in promoting and controlling exsolved nanoparticle formation. Moreover, the interplay between exsolved nanoparticles and the oxide support plays a critical role in determining the catalytic performance (7). Recent findings have shown that exsolution-induced strain and generation of oxygen and cation vacancies in the host oxide can result in improved oxygen mobility and redox properties (6–8). Nevertheless, the pathways and mechanisms governing controlled exsolution remain poorly understood, especially in systems beyond perovskites (6,9).

High-entropy oxides (HEOs) present an ideal platform for versatile and controlled nanoparticle exsolution. Their exceptional chemical flexibility could allow for the exsolution of more complex alloyed nanoparticles, such as binary and ternary systems (1,10). Furthermore, HEOs have





a high tolerance for defects (11) and internal strain (12), both of which facilitate the exsolution process (4,13), enhance ion transport within the crystal lattice, and improve oxygen mobility (6–8). Moreover, HEOs are known for their sluggish diffusion behavior (14), which mitigates nanoparticle growth at high temperatures, a key limitation for nanocatalysts under reaction conditions. This class of materials presents a versatile platform for designing compositionally complex catalysts, which can be precisely tailored to improve the activity and selectivity of CO₂ hydrogenation to methanol.

It has been demonstrated that Co, Ni, and Cu metallic sites are promising metallic sites for methanol synthesis using the CO₂ hydrogenation reaction. Thus, in this work, we have investigated a HEO spinel composed of (Co_{0.33}Ni_{0.33}Cu_{0.33})(Cr_{0.5}Mn_{0.5})₂O₄. Reducing thermal pretreatments were conducted to tune the exsolution composition of embedded Co, Ni, and/or Cu nanoparticles from 300 to 700 °C. A comprehensive set of local- to longrange structural characterization techniques was employed to elucidate the relationship between structure and catalytic performance in the CO₂ hydrogenation reaction to methanol.

Experimental

Synthesis of high-entropy spinel

 $(Co_{0.33}Ni_{0.33}Cu_{0.33})(Cr_{0.5}Mn_{0.5})_2O_4$ HEO spinel synthesis was conducted employing a sol–gel method (15). Briefly, an acidic solution was prepared by mixing 1.5 mL of HNO₃ in 26 mL of deionized water, followed by the addition of 0.6 g of D-sorbitol (used as complexing agent). A total of 2.5 mmol of the desired metals, in the form of nitrates, were then dissolved into the solution. The solution was stirred and heated in a bath at 90 °C for 2 h to form a homogeneous gel, which was then dried at 200 °C overnight. The resulting material was ground and calcined at 700 °C. Reducing thermal pre-treatments were conducted in a continuous tubular reactor (quartz tube, inner diameter of 8 mm) using 5% H₂/He with a total flow of 100 mL min⁻¹ for 10 min at temperatures ranging from 300 to 700 °C.

Characterization

Textural, structural, and electronic characterizations of the catalysts were conducted using various techniques, such as N₂ physisorption, powder X-ray diffraction (PXRD), pair distribution function (PDF) analysis, X-ray photoelectron spectroscopy (XPS), high-resolution scanning transmission electron microscopy (HR-STEM) coupled to energy dispersive X-ray spectroscopy (EDS), and temperature programmed reduction (TPR). *In situ* PXRD, PDF, and near ambient pressure XPS (NAP-XPS) during the exsolution process were also conducted.

CO₂ hydrogenation catalytic evaluation

CO₂ hydrogenation tests at high pressure were conducted in a 10 mL stainless steel batch reactor. The reactor was pressurized with 70 bar using a gas mixture of 76%H₂/19%CO₂/5%N₂ (H₂/CO₂ ratio = 4), sealed, and heated to 200 °C, achieving a final pressure of 100 bar. The reaction was carried out for 20 h. The reactor was cooled down, and the gaseous products analyzed *via* gas chromatography using a thermal conductivity detector. Water-soluble products (*e.g.*, alcohols) were collected in ultrapure water and analyzed *via* gas chromatography using a flame ionization detector. The product distribution, conversion, and yield were calculated to compare the catalytic performances of the catalysts.

Results and Discussion

Structural and electronic evolution during exsolution

We have synthesized (Co_{0.33}Ni_{0.33}Cu_{0.33})(Cr_{0.5}Mn_{0.5})₂O₄ HEO in a spinel structure (AB₂O₄), following a sol-gel method. The use of sugars in sol-gel syntheses is a promising approach for HEOs, as their hydroxyl groups act as coordination centers for the metal cations, ensuring a homogeneous distribution of multiple metal species and preventing phase segregation during the gelation and crystallization process. PXRD measurements were conducted to confirm the formation of single-phase spinel oxide after calcination. The exsolution process, in which the A site metals partially or completely leave the spinel lattice, was tracked in detail by *in situ* time-resolved PXRD (Figure 1a) under a reducing atmosphere. We were able to verify that during heating, the formation of metallic face-centered

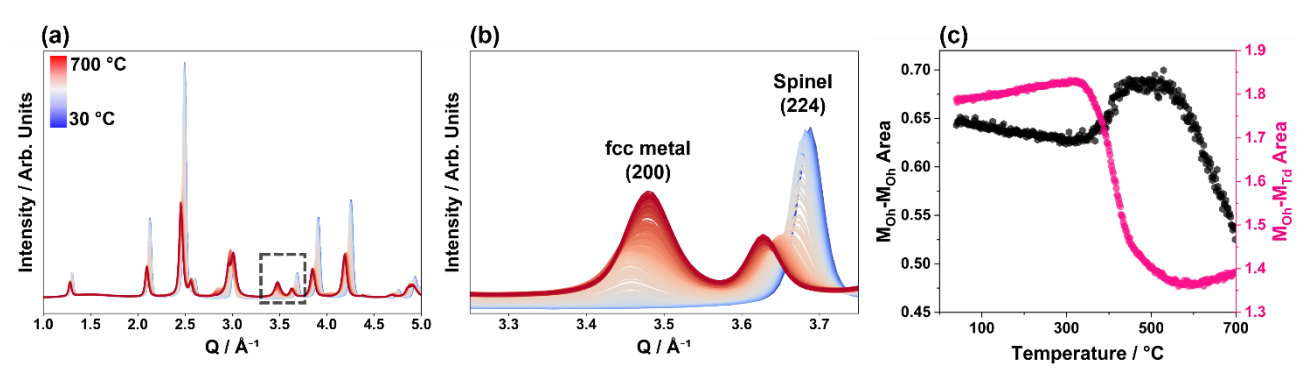


Figure 1: (a) in situ PXRD patterns of (Co_{0.33}Ni_{0.33}Cu_{0.33})(Cr_{0.5}Mn_{0.5})₂O₄ upon heating under reducing atmosphere, (b) zoomed region highlighted in (a), (c) metal-metal atomic pairs octahedra and tetrahedra connectivity correlation with increasing temperature under reducing atmosphere obtained by PDF data analysis.





cubic (fcc) reflections occurred at temperatures above 350 °C. Further heating, up to 700 °C, led to an increase in intensity and shifts to greater Q values (Figure 1b), indicating the formation of a higher number of crystallites and their unit cell shrinkage, respectively. Concomitant to the formation of crystalline fcc metallic nanoparticles, it was possible to observe the spinel reflections decreasing in intensity, shifting to lower Q values, and becoming broader. These changes in the PXRD patterns suggest that part of the metals were segregated from the spinel lattice, resulting in vacant metallic sites (i.e., lower number of scatterers) and increased lattice strain. These observations align with the exsolution of the metals from the spinel lattice and the formation of embedded nanoparticles. Figure 1b shows a zoom of the region highlighted in Figure 1a, facilitating the visualization of these structural changes on the PXRD data as a function of temperature.

Qualitative PDF analysis of the octahedra (Oh) and tetrahedra (Td) building blocks connectivity of the spinel lattice provided information on the short-range order structure (Figure 1c). The peaks at *ca.* 2.9 Å and 3.5 Å are assigned to the metal-metal (M-M) pairs with Oh-Oh (black symbols) and Oh-Td (pink symbols) connectivity, respectively. During the exsolution process, the number of M_{Oh}-M_{Td} pairs starts decreasing at *ca.* 350 °C, until reaching *ca.* 600 °C. On the other hand, M_{Oh}-M_{Oh} pairs start

increasing at ca.350 °C, reaching a plateau at ca.450 °C, and decreasing steadily from ca.550 to 700 °C. These local structure modifications demonstrate that the exsolved metals initially leave the Td sites with concomitant rearrangement of the spinel lattice by the increase in Oh coordination. At higher temperatures, the metals also exsolve from the Oh sites.

To further validate these observations, the sample was pre-treated under reducing atmosphere at 400, 500, and 700 °C for 10 min, and measured using HR-STEM coupled to EDS (Figure 2). The images evidenced the exsolution of small nanoparticles (<10 nm) mainly composed of Cu at 400 °C (Figure 2a-d). Reducing at 500 °C also induced the partial exsolution of Ni and Co, in which a Cu core and Ni/Co shell configuration was obtained (Figure 2e-h). Further heating to 700 °C resulted in particle growth (up to ca. 25 nm) and the formation of a CuNiCo trimetallic alloy (Figure 2i-l).

NAP-XPS measurements under a reducing atmosphere of the same sample were also explored (not shown). The spectra confirmed the surface restructuration of the sample under reducing atmosphere: the exsolution of Cu began at 300 °C, followed by Ni at 400 °C, and Co at 500 °C. At 700 °C Cu, Ni, and Co spectra presented a metallic profile, consistent with that observed by HR-STEM/EDS.

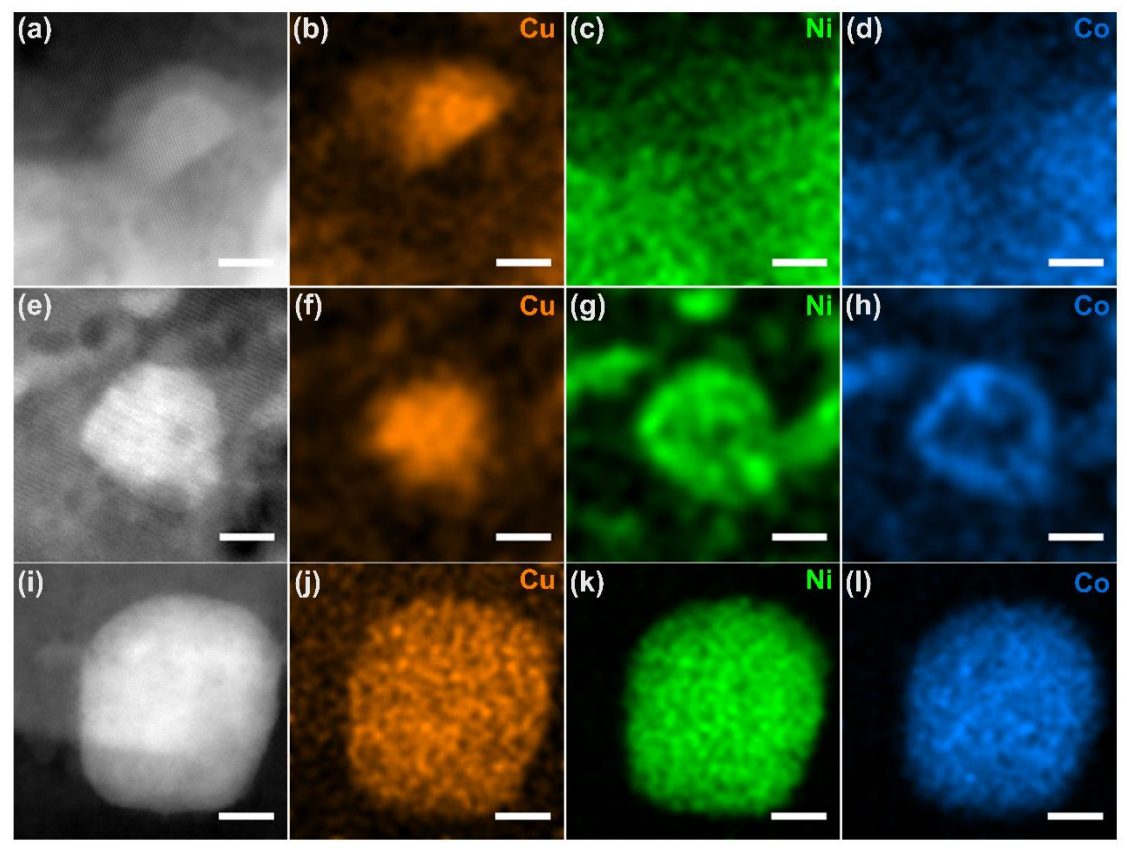


Figure 2: Representative HR-STEM images and respective Cu, Ni, and Co EDS maps of $(Co_{0.33}Ni_{0.33}Cu_{0.33})(Cr_{0.5}Mn_{0.5})_2O_4$ reduced at (a-d) 400 °C, (e-h) 500 °C, and (i-l) 700 °C. Scale bar of 5nm.





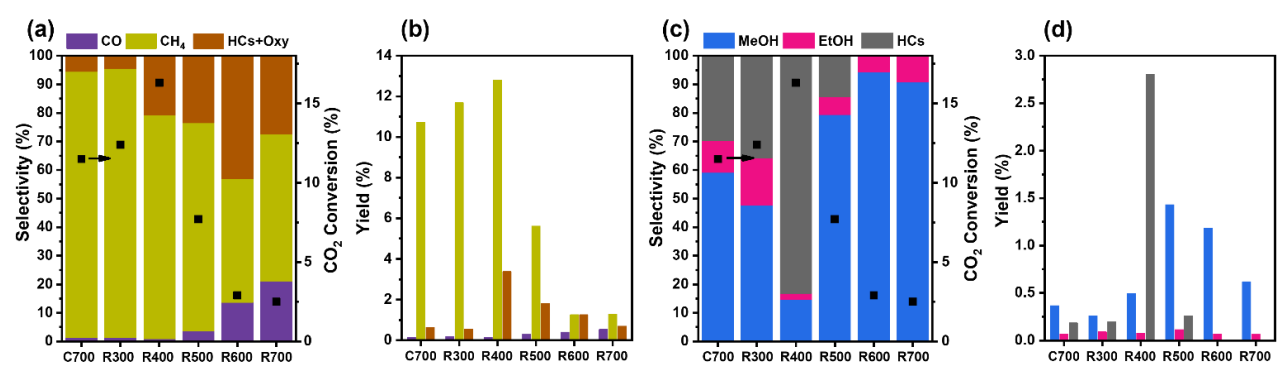


Figure 3: CO_2 hydrogenation catalytic tests employing $(Co_{0.33}Ni_{0.33}Cu_{0.33})(Cr_{0.5}Mn_{0.5})_2O_4$ pre-treated under reducing atmosphere at different temperatures (300 to 700 °C). Selectivity of (a) CO, CH₄, and hydrocarbons (HCs) and oxygenates (Oxy) and (c) HCs + Oxy fraction segmented into MeOH, EtOH, and HCs; (b) and (d) represent the Yields of (a) and (c), respectively. Reaction conditions: 100 bar, 200 °C, 20 h, H_2/CO_2 = 4, 50 mg catalyst. C stands for calcined and R for reduced.

*CO*₂ hydrogenation catalytic evaluation

The catalyst with different reducing thermal pretreatments (i.e., Rx, where 300°C<x<700 °C) was evaluated in the CO₂ hydrogenation reaction at 100 bar and 200 °C for 20 h, and the results are presented in Figure 3. Initially, the catalyst was tested without any reducing pre-treatment (i.e., calcined at 700 °C, C700), resulting in a CO2 conversion of 11.5 % and favoring the formation of CH₄ (93.3%), with CO and HCs+Oxy representing 1.3% and 5.4%, respectively. The R300 catalyst presented similar catalytic performance to C700. By increasing the reduction temperature to 400 °C (i.e., R400), increases in the CO₂ conversion (16.3%) and HCs+Oxy selectivity (20.7%) occurred. For samples reduced at higher temperatures (R500-R700), although the selectivity for HCs+Oxy (up to 2.1-fold) and CO (up to 23.5-fold) continued to increase, the CO₂ conversion dropped drastically (up to 6-fold), leading to much lower overall product yields. A maximum of HCs+Oxy selectivity was achieved at 600 °C, representing 43.1%.

A more detailed analysis of the HCs+Oxy products (Figure 3c-d) revealed that methanol was the major product among the oxygenates, particularly in samples R500 to R700, which presented high selectivities (*ca.* 80-94%). While R600 and R700 did not form HCs, R500 presented the highest methanol yield among all catalysts. The high selectivity and yield towards HCs for R400 should also be highlighted.

A clear trend in selectivity is observed, suggesting that the composition of exsolved nanoparticles plays a direct role in the reaction pathway. In particular, one can notice that the CuNiCo alloyed nanoparticles (*i.e.*, R600 and R700) were highly selective towards MeOH. However, the excessive reduction led to particle growth and a decrease in activity. Moreover, the best compromise between activity and selectivity towards methanol was accomplished by R500 catalyst, achieving the greatest methanol yield (*ca.* 1.5 %).

Conclusions

In summary, we demonstrated that the exsolution of multimetallic nanoparticles from a high-entropy spinel oxide can be finely tuned by controlling the reduction temperature, directly impacting the catalytic performance in hydrogenation reaction. Structural the CO₂ spectroscopic analyses revealed a temperature-dependent exsolution pathway in which Cu, Ni, and Co are sequentially exsolved, forming compositionally distinct nanoparticles ranging from monometallic Cu to trimetallic CuNiCo alloys. Moderate reduction at 500 °C led to the formation of dispersed and catalytically active particles, maximizing methanol yield and selectivity. In contrast, excessive reduction at higher temperatures (≥600 °C) resulted in particle growth, surface restructuring, and a loss of CO₂ conversion despite higher selectivity to alcohols. These findings underscore the potential of HEOs as tunable platforms for generating multimetallic interfaces and open new perspectives for designing stable and efficient catalysts for CO₂ hydrogenation to methanol.

Aknowledgements

We are grateful for funding from the Villum Foundation (VKR00042079), Carlsberg Foundation (CF21-0278), Danish Ministry of Higher Education and Science (SMART Lighthouse), Danish National Research Foundation Center for High-entropy Alloy Catalysis (DNRF 149), European Research Council (804066), Fundação de Amparo à Pesquisa do Estado de São Paulo (FAPESP, 2018/01258-5, 2020/12986-1, 2023/02561-1), Conselho Nacional de Desenvolvimento Científico e Tecnológico (CNPq, 311226/2022-1, 405800/2022-3, and 409401/2023-4), and Coordenação de Aperfeiçoamento de Pessoal de Nível Superior (CAPES finance code 001).



SBCAT SOCIEDADE BRASILEIRA DE CATÁLISE

References

- (1) Najimu, M.; Jo, S.; Gilliard-AbdulAziz, K. L. Co-*Acc Chem Res* **2023**, *56* (22), 3132–3141.
- (2) Kim, J. H.; Kim, J. K.; Liu, J.; Curcio, A.; Jang, J. S.; Kim, I. D.; Ciucci, F.; Jung, W. C. *ACS Nano*. American Chemical Society January 26, 2021, pp 81–110.
- (3) Zhang, M.; Gao, Y.; Xie, C.; Duan, X.; Lu, X.; Luo, K.; Ye, J.; Wang, X.; Gao, X.; Niu, Q.; Zhang, P.; Dai, S. *Nat Commun* **2024**, *15* (1), 8306.
- (4) Kousi, K.; Tang, C.; Metcalfe, I. S.; Neagu, D. *Small.* John Wiley and Sons Inc May 1, 2021.
- (5) Shi, Y. F.; Ma, S.; Liu, Z. P. *EES Catalysis* **2023**, *1* (6), 921–933.
- (6) Sun, Z.; Hao, C.; Toan, S.; Zhang, R.; Li, H.; Wu, Y.; Liu, H.; Sun, Z. Royal Society of Chemistry August 3, 2023, pp 17961–17976.
- (7) Wang, J.; Kumar, A.; Wardini, J. L.; Zhang, Z.; Zhou, H.; Crumlin, E. J.; Sadowski, J. T.; Woller, K. B.; Bowman, W. J.; Lebeau, J. M.; Yildiz, B. *Nano Lett* **2022**, *22* (13), 5401–5408.
- (8) Su, C.; Wang, W.; Shao, Z. Acc Mater Res **2021**, *2* (7), 477–488.
- (9) Weber, M. L.; Šmíd, B.; Breuer, U.; Rose, M. A.; Menzler, N. H.; Dittmann, R.; Waser, R.; Guillon, O.; Gunkel, F.; Lenser, C. *Nat Mater* **2024**, *23* (3), 406–413.
- (10) Luo, Y.; Chang, X.; Wang, J.; Zhang, D.; Fu, L.; Gu, X. K.; Wang, Y.; Liu, T.; Ding, M. *ACS Nano* **2025**, *19* (1), 1463–1477.
- (11) Zhao, B.; Du, Y.; Yan, Z.; Rao, L.; Chen, G.; Yuan, M.; Yang, L.; Zhang, J.; Che, R. *Adv Funct Mater* **2023**, *33* (1).
- (12) Han, Y.; Liu, X.; Zhang, Q.; Huang, M.; Li, Y.; Pan, W.; Zong, P. an; Li, L.; Yang, Z.; Feng, Y.; Zhang, P.; Wan, C. *Nat Commun* **2022**, *13* (1).
- (13) Han, H.; Park, J.; Nam, S. Y.; Kim, K. J.; Choi, G. M.; Parkin, S. S. P.; Jang, H. M.; Irvine, J. T. S. *Nat Commun* **2019**, *10* (1).
- (14) Kodama, K.; Nagai, T.; Kuwaki, A.; Jinnouchi, R.; Morimoto, Y. *Nature Nanotechnology*. Nature Research February 1, **2021**, pp 140–147.
- (15) Kirsch, A.; Bøjesen, E. D.; Lefeld, N.; Larsen, R.; Mathiesen, J. K.; Skjærvø, S. L.; Pittkowski, R. K.; Sheptyakov, D.; Jensen, K. M. Ø. *Chemistry of Materials* **2023**, *35* (20), 8664–8674.